

# A Novel Flash Photolysis/UV Absorption System Employing Charge-Coupled Device (CCD) Detection: A Study of the BrO + BrO Reaction at 298 K

David M. Rowley,\* Matthew H. Harwood, Raymond A. Freshwater, and Roderic L. Jones

Centre for Atmospheric Science, University Chemical Laboratory, Lensfield Road, Cambridge CB2 1EW, U.K.

Received: July 6, 1995; In Final Form: September 25, 1995<sup>⊗</sup>

A novel flash photolysis/kinetic absorption spectroscopy system has been constructed for the study of gas phase reactions. The experiment incorporates a charge-coupled device (CCD) detector and represents the first application of such devices to the study of gas phase kinetics. The CCD enables the recording of rapid sequential time-resolved UV/visible absorption spectra before, during, and after photolysis of a gas mixture. The unequivocal identification and monitoring of several absorbing components in the reacting mixture is therefore possible, thereby maximizing the amount of information gathered from a single flash photolysis experiment. The experimental system is described in full here. Results from a preliminary kinetic study of the BrO self-reaction at 298 K are also described:  $\text{BrO} + \text{BrO} \rightarrow 2\text{Br} + \text{O}_2$  (1a);  $\text{BrO} + \text{BrO} \rightarrow \text{Br}_2 + \text{O}_2$  (1b). Experiments were performed to independently determine the rates of the overall reaction,  $k_1$ , defined by  $(-d[\text{BrO}]/dt = 2k_1[\text{BrO}]^2)$  and both individual reaction channels (1a) and (1b), giving  $k_1 = (2.98 \pm 0.42) \times 10^{-12} \text{ cm}^3 \text{ molecule}^{-1} \text{ s}^{-1}$ ;  $k_{1a} = (2.49 \pm 0.42) \times 10^{-12} \text{ cm}^3 \text{ molecule}^{-1} \text{ s}^{-1}$ ; and  $k_{1b} = (4.69 \pm 0.68) \times 10^{-13} \text{ cm}^3 \text{ molecule}^{-1} \text{ s}^{-1}$  at 298 K and 760 Torr total pressure in oxygen bath gas. Errors are  $2\sigma$ . Deviations from the expected second-order kinetic scheme were observed in the experimental system wherein bromine was photolyzed in the presence of excess ozone as a source of the BrO radicals. At low ozone concentrations, the formation of Br<sub>2</sub>O is proposed, and at very high ozone concentrations the formation of symmetric bromine dioxide, OBrO, is observed. Kinetic schemes for these side reactions have been deduced, and the mechanistic implications of these results are discussed.

## Introduction

Of the available laboratory techniques for the study of gas phase reactions, flash photolysis coupled with kinetic absorption spectroscopy has proved to be one of the most powerful. The technique, originally developed in this laboratory in the 1950s,<sup>1,2</sup> involves the rapid generation of reactive species, atoms and free radicals, which are then monitored, by virtue of their characteristic UV/visible absorptions, as a function of time. The nature and rates of reactions involved in their removal are then inferred from the decay trace obtained. Since its conception, refinements to the flash photolysis technique have come about as a result of technical improvements, particularly in the monitoring of transient absorptions.

In the original flash photolysis experiments, photographic plates were used to measure absorptions.<sup>1,2</sup> The plate was situated in the dispersive plane of a spectrograph, and the light intensity from a pulsed analysis lamp was transmitted through the reaction cell at a given delay time after the photolysis flash and recorded. The wavelength-resolved signals were converted manually into absorptions by measuring the degree of darkening across the photographic plates. Repeated experiments using different delay times between the photolysis and the analysis flash were then carried out to build up the temporal profile of the absorption.

With the advent of electronic photodetectors, photomultiplier tubes (PMTs), the absorption signal from a flash photolysis experiment could be monitored continuously as a function of time.<sup>3</sup> This enabled the recording of a decay trace in a single experiment. However, because of the size of the PMT and the inability of the detector to discriminate light falling on different

parts of the detector window, simultaneous wavelength-resolved measurements were not possible. Thus, the PMT allowed the monitoring of a single wavelength of analysis light which was selected using a monochromator. Use of a single wavelength limited the ability to identify species, however, and no discrimination between other absorbers was possible. Despite this, the electronic recording of intensity and the use of more stable continuous analysis lamps have greatly improved the reliability of detection over that obtained from the use of photographic plates, and photomultiplier tubes are still widely used in flash photolysis systems today (*e.g.* refs 4, 5).

Recently, the availability of photodiode arrays has enabled the monitoring of analysis light intensity electronically and simultaneously as a function of both wavelength and time. The array consists of a row of small, separate light sensitive elements which can be aligned along the dispersive axis of a spectrograph. The time resolution of the recording is limited by the readout time of the device. Since readout takes place sequentially for each element of the array, full readout takes typically milliseconds, and diode arrays are therefore unsuitable for the study of fast kinetic processes. Nevertheless, photodiode arrays have proved useful in the study of UV/visible absorption spectra,<sup>6</sup> in studies of slower kinetics, and for product analyses.<sup>7</sup> In addition, fast electronic time gating of photodiode arrays has enabled the recording of short exposure spectra at specific times in a flash photolysis experiment, and, analogously to the photographic plates method, repeated experiments can be performed to build up the full temporal variation of absorption.<sup>5</sup>

In this work a two-dimensional detector array has been incorporated into a flash photolysis system. These arrays, known as charge-coupled devices (CCDs), convert incident light into photocharge and also have the facility to rapidly and efficiently transfer this signal into a storage region on the device. This enables the recording of many sequential spectra at rapid

\* Author to whom correspondence should be addressed. E-mail: rowley@atm.ch.cam.ac.uk.

<sup>⊗</sup> Abstract published in *Advance ACS Abstracts*, January 15, 1996.

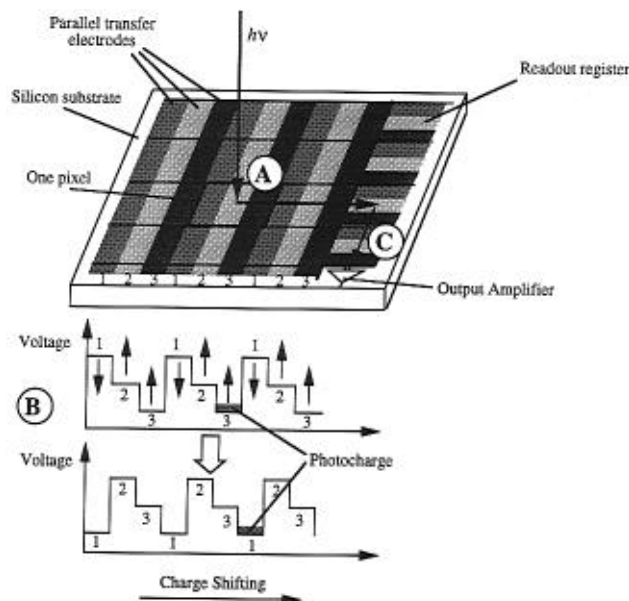


**Figure 1.** Schematic diagram of the principles of CCD operation. Incident light is converted into photocharge (A) and stored in a potential well on the silicon. Three sets of parallel transfer electrodes (1, 2, and 3) are then charged cyclically to maintain a potential gradient across the device and push the photocharge from pixel to pixel (B). Finally, when photocharge from the first pixel has traversed the whole device, the charge is read out from the readout register to the output amplifier (C).

rates. Thus, the advantage of recording a range of wavelengths of absorption as with a diode array is preserved, without compromising the ability to monitor rapidly and continuously as with a PMT.

**Principles of CCD Operation.** A full account of the theory and operation of charge-coupled devices<sup>8</sup> is outside the scope of this work. A brief summary of the main features of the CCD is given here.

The charge-coupled device consists of a grid of linearly coupled metal oxide semiconductor (MOS) elements (pixels) embedded in a silicon substrate. These elements convert incident light into photocharge, which is stored in a potential well within the pixel. Transfer of the photocharge from one row of pixels to the adjacent row can then be effected, along one of the axes of the array, by applying suitably phased voltages to parallel electrodes running across each row of pixels. When the charge from the first row has traversed the entire device, readout of each row of pixels can take place on a slower time scale. A schematic diagram of a charge-coupled device is shown in Figure 1, along with the principle of operation of charge transfer.

The quantum efficiency (QE) of the CCD light-to-charge conversion peaks at 700 nm, where  $QE \approx 60\%$ . At lower wavelengths, this efficiency decreases, and for detection at wavelengths below 400 nm, the device is thinly coated with phosphor, which fluoresces at visible wavelengths. Using this coating, the effective QE is *ca.* 20% from 180 to 400 nm. The phosphor fluorescence lifetime is on the order of nanoseconds, and the phosphor coating is extremely thin (0.3  $\mu\text{m}$ ) compared to the pixel size (22.5  $\mu\text{m}$  square). Thus, cross talk between pixels on the device is negligible. The charge transfer efficiency of the CCD is very high, typically  $>(1-10^{-6})/\text{transfer}$ , and rates of charge transfer up to 1 MHz per row of pixels (a 1  $\mu\text{s}$  row-shifting time) are readily attainable. Alternatively, the charge transfer time can be made arbitrarily long.

As with diode arrays, CCDs produce a dark current, which is minimized by Peltier cooling of the device to 200 K and

enclosing it in a vacuum for thermal insulation. This dark signal is recorded for each pixel prior to every readout of the device and subtracted from the measured intensity. Additionally, although a number of potential sources of noise exist in CCD operation, the main source of noise is photonic noise, inherent to the light incident on the device. For a typical full pixel capacity of  $2 \times 10^6$  photoelectrons, this corresponds to a noise level of  $\pm 0.07\%$ .

**Use of a CCD in Flash Photolysis.** The charge-coupled device is used in the flash photolysis system to record rapid sequential spectra of the analysis light transmitted through the reaction mixture before, during, and after photolysis. A schematic of the arrangement is shown in Figure 2. The analysis light collimated through the reaction vessel is imaged across rows at the top of the charge-coupled device, and charge transfer processes are used to record spectra as a function of time. The flash photolysis system is discussed in detail below.

## Experimental Section

Gases are manipulated using a standard Pyrex line equipped with greaseless Teflon taps (Young & Co.). The line consists of two parts: a vacuum line and a gas-mixing line. In the vacuum line, pressures down to  $10^{-5}$  mbar are readily attainable using a rotary/diffusion pump combination and measured using a Pirani/cold cathode detector combination (MKS Instruments Ltd. 953). The gas-mixing line consists of a carrier gas flow tube and five gas injectors aligned against the carrier flow for efficient gas mixing. All gas flows into the mixing line are controlled by mass flow controllers (MKS 1159B).

The reaction cell into which gases are passed is made in Spectrosil quartz tube and is 1 m in length. The cell is double jacketed: the inner jacket containing flowing liquid (Galden HT90) from a recirculating thermostating unit (Huber HS 80). The outer jacket is held at low pressure to prevent condensation on the cell walls when operating at low temperatures. Similarly, double-windowed, evacuated end pieces are used to prevent condensation on optical surfaces. The gas temperature in the cell is monitored using a ceramic enclosed, fast reacting Pt-100 resistance thermometer (Thermospeed PQ 93870), which resides in the gas flow. The gas temperature in the cell is thus controllable from 193 to 373 K within an accuracy of  $\pm 0.5$  K.

Radicals are generated in the cell using flashlamp photolysis. The lamp used is a 1 m arc length xenon lamp, filled to 50 Torr (Qarc Ltd. QDX 66). The lamp is powered from a 25 kV, 2.6  $\mu\text{F}$  rapid discharge capacitor (NWL Ltd.) typically charged to 20 kV using a high-voltage power supply (Glassman High Voltage Ltd. EH100). Since the high voltage used for the lamp would cause self-breakdown and uncontrolled lamp firing if applied directly, a spark gap (EG&G GP12B) is used to hold off the high voltage until lamp triggering. The spark gap is ionized using a trigger unit (EG&G TM11A), itself controlled using an optically isolated TTL (+5 V) pulse from the control computer. The flashlamp circuit is designed to be critically damped to give the maximum efficiency, short pulse duration, and absence of current reversal ("ringing"). The method of Markiewicz and Emmet<sup>9</sup> was used to determine the optimum *R*, *L*, and *C* parameters. The flashlamp pulse energy, approximately 500 J, is completely discharged in less than 20  $\mu\text{s}$ . The optical pulse duration from the flashlamp was measured using a rapid response photodiode and storage oscilloscope and found to be *ca.* 10  $\mu\text{s}$  fwhm. The spectral output of the xenon flashlamp was not measured but, in common with similar lamps operated under analogous conditions, is expected to cover the UV/visible range from 180 to 700 nm.<sup>10</sup>

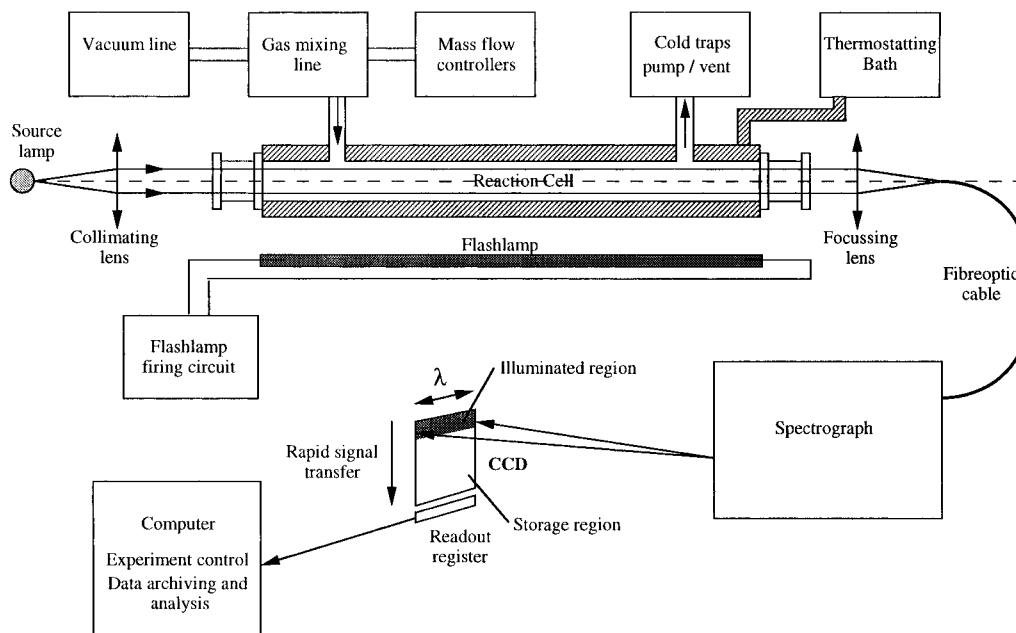


**Figure 2.** Schematic diagram of the flash photolysis system. Light from the source lamp is collimated through the reaction cell and transferred to the spectrograph. Wavelength dispersed light is imaged across the top of the CCD perpendicular to the axis of fast charge transfer. Sequential spectra of the cell contents are recorded by charge transfer on the CCD.

The flashlamp is situated adjacent and parallel to the reaction cell and can be moved toward and away from the reaction vessel (3–10 cm separation) to vary the effective photolysis intensity. When very short (<280 nm) wavelength photolysis is not required, the flashlamp is enclosed in a Pyrex envelope. A slow flow of air through this envelope cools the lamp and prevents ozone buildup from atmospheric photolysis around the lamp.

The reaction cell and flashlamp are enclosed in a light-tight metal box. The box is baffled to minimize the escape of flashlamp light along the optical axis and earthed to minimize radiofrequency interference from the flashlamp. Similarly, the flashlamp circuit is enclosed in a Faraday cage, earthed to the same point. All electrical leads into the flashlamp circuit are screened, and main power is supplied from a filtered unit, incorporating an earth choke.

Radicals and molecules in the reaction cell are identified and monitored by virtue of their UV/visible absorption. The source is a 30 W high-brightness deuterium lamp (Hamamatsu L5499) for use in the UV or a 30 W continuous xenon arc lamp (Applied Photophysics Ltd.) for visible output. The lamp output is collimated through the cell and focused, using a pair of 100 mm focal length Spectrosil quartz lenses (Comar Ltd.), onto a 550  $\mu\text{m}$  diameter fused silica optical fiber (Ensign-Bickford). The fibre is  $f$ -matched and coupled to a 250 mm focal length astigmatic Czerny-Turner spectrograph (Chromex 250IS) which images the dispersed light onto the CCD.

The spectrograph is equipped with three interchangeable diffraction gratings, ruled at 150, 300, and 600 grooves/mm, giving spectral coverages of *ca.* 120, 60, and 30 nm, respectively. The corresponding limiting spectra resolutions of each grating were *ca.* 0.45, 0.22, and 0.11 nm fwhm, respectively. The instrument function of the spectrograph was recorded for each grating at a range of slit widths from 10 to 1000  $\mu\text{m}$ . Each grating was periodically wavelength and dispersion calibrated using lines emitted from a low-pressure mercury lamp.

The maximum temporal resolution between successive spectra recorded with the CCD is determined by the minimum charge shift time of the device and the size of the image of the analysis UV/visible source at the detector in the axis of fast charge

transfer. The latter is minimized by the use of a small source (the fiber-optic cable) and an astigmatic, imaging spectrograph. This preserves the vertical integrity of the source to a much greater extent than normal Czerny-Turner designs, by virtue of toroidal collimating and focusing mirrors and, with the small image size, thereby maximizes temporal resolution.

The optical fiber diameter used is 550  $\mu\text{m}$ , and after magnification by the spectrograph the height of the image corresponds to 35 pixels (pixels are 22.5  $\mu\text{m}$  square) at the detector. Thus, using the detector's minimum shift time of 9  $\mu\text{s}/\text{row}$ , a single row of spectral data takes a minimum of 315  $\mu\text{s}$  to acquire. This spectral acquisition time can be further reduced, at the expense of light throughput, by the use of a smaller diameter (100  $\mu\text{m}$ ) optical fiber.

The CCD used is a UV coated 298  $\times$  1152 pixel sensor (EEV CCD05-10-0-202), mounted in a Peltier cooled camera head (Wright Instruments Ltd.). The device is oriented with the 298 pixel axis in the dispersive plane of the spectrograph. The camera is coupled to the spectrograph with a flange which allows linear motion in two axes for focusing and vertical translation of the CCD with respect to the spectrograph output. A baffle is situated on the window of the detector to minimize the levels of scattered light falling onto the storage region of the CCD. A shutter in the camera head is also used, to prevent buildup of photocharge on the device between experiments.

The spectrograph, camera, and triggering are all controlled from a personal computer. Data files of the transmitted intensity as a function of wavelength and time are recorded on this computer, archived onto data storage tape, and transferred to a separate personal computer for analysis. Two types of spectral analysis are performed: spectra of gas mixtures in the cell without photolysis are recorded by ratioing equivalent accumulated columns of pixels from successive CCD exposures with and without the gas mixture, and applying Beer's law:

$$A_{\lambda} = \ln(I_{o,\lambda}/I_{g,\lambda}) \quad (i)$$

wherein  $A_{\lambda}$  is the absorbance of the gas mixture at a given wavelength  $\lambda$ ,  $I_{o,\lambda}$  is the total intensity recorded by a column of

pixels in the absence of the gas mixture, and  $I_{g,\lambda}$  is the intensity recorded with the gas mixture in the cell.

For kinetic (flashed) experiments, Beer's law is applied similarly, but with  $\langle I_{o,\lambda} \rangle$  as an average intensity recorded in the preflash period and  $I_{g,\lambda,t}$  that recorded for each pixel recorded at a time  $t$  after the photolysis flash.

$$A_{\lambda,t} = \ln(\langle I_{o,\lambda} \rangle / I_{g,\lambda,t}) \quad (\text{ii})$$

wherein  $A_{\lambda,t}$  is the absorption relative to the preflash intensity at a wavelength  $\lambda$  and time  $t$  after the photolysis flash. Spectra therefore represent changes in the absorptions caused by the photolysis flash as a result of reactant consumption and radical formation. Sequential spectra show the temporal evolution of these changes.

Analysis of the measured absorption spectra to determine the concentrations of the expected absorbers was carried out by numerically fitting reference cross sections of these species to the experimental spectra. In this process, the Beer-Lambert law is used to construct a simulated spectrum from a linear combination of the expected absorbances:

$$B_{\lambda} = \alpha \sigma_{A,\lambda} + \beta \sigma_{B,\lambda} + \dots \quad (\text{iii})$$

wherein  $\alpha = l[A]$ ;  $\beta = l[B]$ ;  $B_{\lambda}$  is the simulated absorption at wavelength  $\lambda$ ;  $\sigma_{A,\lambda}$ ,  $\sigma_{B,\lambda}$ , ... are the absorption cross sections for species A, B, ..., respectively; and  $l$  is the optical path length. This spectrum is then fitted to the experimental spectrum by minimizing the sum of squares of the difference between the simulated and experimental spectra with respect to the coefficients  $\alpha$ ,  $\beta$ , ..., allowing the determination of concentrations  $[A]$ ,  $[B]$ , .... Often, spectral regions can be chosen such that individual absorptions show little overlap and simple scaling of reference spectra in spectral regions exclusive to that absorber can be used to determine its concentration.

If a spectral contribution is structured, a differential technique can be used to determine the concentration of the structured absorber in the presence of other smooth absorptions. Briefly, this involves fitting a function to the smooth shape of the composite absorption and subtracting this expression to leave the spectral structure alone: the differential spectrum. The reference spectrum is then treated similarly, and the reference differential is fitted to the observed differential using linear least-squares techniques as described above. The differential spectrum may also be shifted by small increments in the wavelength axis, to optimize the fit of the reference spectrum and account for any small deviations in the wavelength calibration.

The reference spectra for absorbing species used in the spectral stripping processes are either recorded or taken from the literature. In the latter case, where required, special care is taken to smooth the literature spectrum to the same wavelength resolution as used in this study. This is particularly important for the structured spectra, where the values of  $\sigma_{\lambda}$  are a strong function of the spectrometer resolution.

Having converted the measured absorptions into species concentration *vs* time data for the species of interest, kinetic analysis is undertaken. In cases where the differential equations governing the temporal variation of measured species are soluble, a classical analysis can be performed. With more complex reaction systems, the commercial software package FACSIMILE<sup>12</sup> is used to numerically integrate the differential equations and fit the observed data to a simulated scheme, allowing the optimization of rate constants. A minor complication to both types of analysis is encountered as a result of the inherent time averaging of data from the CCD, due to the finite vertical extent of the image of the analysis source on the device.

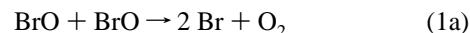
Uncorrected, this leads to small deviations in values returned, compared to those obtained from the "pure" kinetic analysis. Corrections to the analyses were therefore developed and have been applied in both cases. These corrections involve the time averaging of a simulated decay trace, in an identical way to that which occurs optically at the CCD, followed by the fitting of the simulated and averaged decay trace to the observed decay.

An initial kinetic study, carried out to characterize the new system, is described below.

### The BrO Self-Reaction

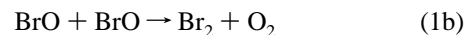
The self-reactions of halogen monoxide (XO) radicals have been studied by many groups using a variety of techniques.<sup>13,14</sup> The reactions have a number of product channels, and the resulting complications in the kinetic analysis of such systems have led to a wide range of different results. The widespread use of UV absorption spectroscopy to monitor the radicals, *via* the characteristic structured ( $A \leftarrow X$ ) absorption, means that some of the discrepancy between results can be attributed to the cross sections used, which are a function of the instrumental resolution. For experiments using PMT detection, single-wavelength monitoring is also susceptible to interferences by underlying absorptions generated in the reaction. As shown by Mauldin *et al.*,<sup>5</sup> the use of diode array spectroscopy enables the specific identification and quantification of halogen monoxide radicals by using the whole structured UV spectrum. In this experiment, sequential absorption spectra are recorded during an experiment, thereby precluding the need to conduct separate experiments for each time-resolved data point.

BrO radicals play important roles in the atmosphere. Catalytic cycles involving BrO are implicated in the observed depletions of stratospheric ozone in polar regions and over midlatitudes. Tropospheric ozone is also affected by bromine oxide chemistry: for example a near-total loss of surface ozone in marine polar regions has been observed, which has been correlated with bromine emissions from phytoplankton.<sup>16</sup> Here, the BrO self-reaction has been directly implicated in the ozone loss mechanism:



Modeling these atmospheric processes therefore requires a knowledge of rate constants for all the channels involved. Furthermore, in the kinetic studies of the halogen oxide cross reactions (*e.g.* BrO + ClO) it is first necessary to fully characterize the self-reactions, as they will also contribute to the observed radical loss in the kinetic experiment.

Previous studies of the BrO self-reaction have shown that two channels exist: one producing atomic bromine (reaction 1a) and the other producing molecular bromine:



Reported values for  $k_1 = k_{1a} + k_{1b}$  are in the range  $(0.66-5.2) \times 10^{-12} \text{ cm}^3 \text{ molecule}^{-1} \text{ s}^{-1}$ .<sup>5,17-25</sup> Channel 1a is considered to be the dominant pathway for the self-reaction of BrO radicals, with both direct and indirect studies<sup>17-25</sup> giving an average  $\alpha = \{k_{1a}/(k_{1a} + k_{1b})\} = 0.85 \pm 0.03$ .<sup>5</sup> Thus, although the partitioning of the two channels is well-established, the overall rate of the self-reaction is less so.

In this study, the self-reaction was studied using two separate sources of BrO radicals. In the first, the short wavelength ( $\lambda$

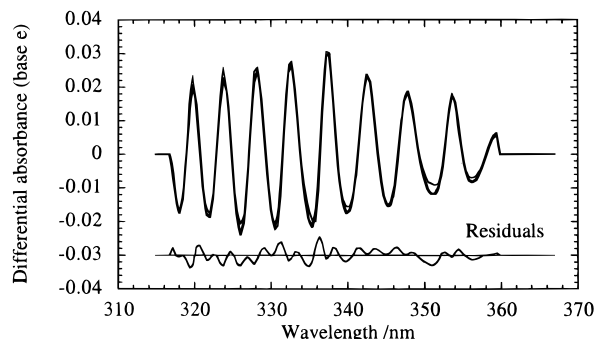


**Figure 3.** Differential fit of a single postflash absorption spectrum (thick line) to the BrO reference spectrum (fine line). The residuals have been offset by  $-0.03$  absorbance units, for clarity. Instrumental resolution =  $1.7$  nm fwhm.

$< 200$  nm) photolysis of molecular oxygen ( $[O_2] = 2.4 \times 10^{19} \text{ cm}^{-3}$ ) in the presence of molecular bromine ( $[Br_2] > 9 \times 10^{16} \text{ cm}^{-3}$ ) was used,



whereas in the second system, the longer wavelength ( $\lambda \approx 400$  nm) photolysis of bromine ( $[Br_2] = (1-5) \times 10^{16} \text{ cm}^{-3}$ ) in the presence of ozone ( $[O_3] = 5 \times 10^{15}$  to  $7 \times 10^{17} \text{ cm}^{-3}$ ) was used,



In both cases, the molecular species was maintained in excess over the photolytically generated atoms, and BrO radicals were formed on a much shorter time scale than their subsequent removal. Initial BrO concentrations varied from *ca.*  $5 \times 10^{13} \text{ cm}^{-3}$  in the oxygen photolysis system to *ca.*  $4 \times 10^{14} \text{ cm}^{-3}$  in the bromine photolysis system, with photolysis flash energies ranging from 470 to 690 J. As discussed below, the use of separate sources for the radicals enabled the direct characterization of both reaction channels.

The BrO radicals were monitored as a function of time using the CCD as described above. Post flash absorbance *vs* wavelength *vs* time traces were recorded over the wavelength range 234–367 nm, at a spectral resolution of 1.7 nm fwhm and for total periods ranging from 60 to 400 ms. Where necessary, the signal-to-noise ratio of the traces was improved by coaddition of up to 15 experiments.

Traces were analyzed for BrO using the absorption cross section values of Wahner *et al.*<sup>26</sup> The spectrum was convolved onto our instrument function using a sliding Gaussian average. This function was chosen, as it gave the best reproduction of our instrument function. A differential spectrum was produced from the convolved BrO spectrum and fitted and stripped from the experimental spectrum in each temporal recording from the CCD. Wavelength shift routines were used to finely match the wavelength calibration of the reference and experimental spectra. A typical fit to the BrO differential spectrum is shown in Figure 3. After removal of the contribution of BrO to the experimental spectra in the bromine/ozone photolysis system, the residual absorbance spectra showed negative absorptions attributed to the consumption of ozone during the experiment. A reference ozone spectrum<sup>27</sup> was therefore used, again convolved to our instrument function, to retrieve the change in ozone concentration as a function of time. Since the ozone spectrum shows no

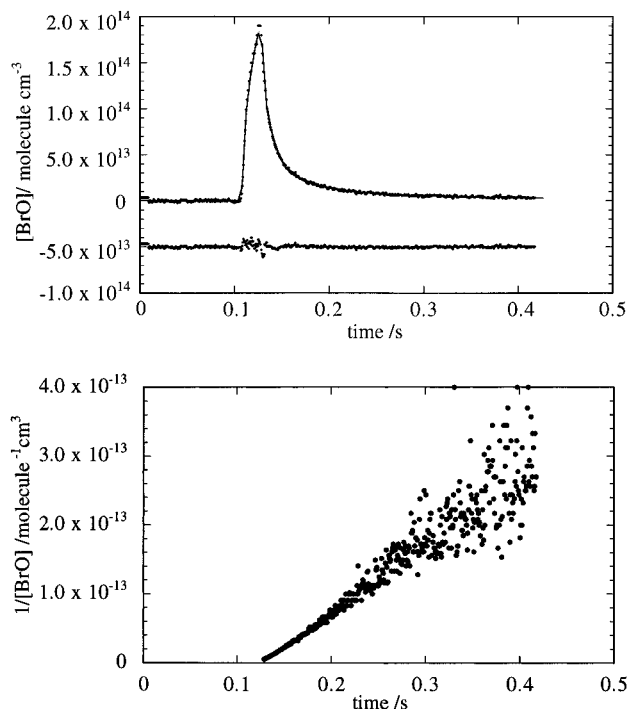


**Figure 4.** (a, top) Typical experimental buildup and decay trace for [BrO] (data points) with best-fit simulated trace from FACSIMILE (solid line). The residuals have been offset by  $-5.0 \times 10^{13}$  molecules  $\text{cm}^{-3}$ , for clarity. (b, bottom) Second-order plot of the postflash data from (a).

spectral structure with sufficiently large differential cross sections in this wavelength region, the retrieval used the tail of the Hartley band to determine the changes in ozone concentration. After adding in the contribution of ozone to the spectra from the bromine/ozone system, the residual spectrum showed no other significant absorbance at any point in the decay trace: the absorption cross sections of bromine are too small over the wavelength range used to show  $Br_2$  consumption. Similarly, in the oxygen photolysis system, no absorbance other than that due to BrO was observed.

## Results/Discussion

Decay traces were recorded under a range of conditions at 298 K and were generally well-described by a second-order kinetic scheme. Thus,

$$\frac{-d[BrO]}{dt} = 2k_{obs}[BrO]^2 \quad (iv)$$

and, integrating,

$$\frac{1}{[BrO]_t} = \frac{1}{[BrO]_0} + 2k_{obs}t \quad (v)$$

A typical decay trace and plot of  $1/[BrO]_t$  *vs*  $t$  are shown in Figure 4. This type of classical kinetic analysis and numerical integration and fitting using FACSIMILE were used to return values of  $k_{obs}$ . The basic reaction scheme used for the numerical integration in FACSIMILE is shown in Table 1.

Values of  $k_{obs}$  were obtained from both chemical systems. In the case of the oxygen photolysis experiments, this value represented the BrO self-reaction through both channels:  $k_{obs} = k_{1a} + k_{1b}$ . In the bromine photolysis system, however, the measured rate constant resulted from channel 1b only, as BrO radicals were rapidly regenerated, *via* reaction 2, from bromine

**TABLE 1: Reaction Scheme Used for Numerical Integration of the BrO + BrO Reaction**

reaction	$k_{(298\text{ K})}/\text{cm}^3 \text{ molecule}^{-1} \text{ s}^{-1}$	reference
$\text{O} + \text{Br}_2 \rightarrow \text{BrO} + \text{Br}^a$	$1.4 \times 10^{-11}$	14
$\text{Br} + \text{O}_3 \rightarrow \text{BrO} + \text{O}_2^b$	$1.2 \times 10^{-12}$	13
$\text{BrO} + \text{BrO} \rightarrow 2\text{Br} + \text{O}_2$	optimized	this work
$\text{BrO} + \text{BrO} \rightarrow \text{Br}_2 + \text{O}_2$	optimized	this work
$\text{Br} + \text{Br} + \text{M} \rightarrow \text{Br}_2 + \text{M}$	$7.6 \times 10^{-14c}$	17

<sup>a</sup> In oxygen photolysis system only. <sup>b</sup> In bromine photolysis system only. <sup>c</sup> At 760 Torr in nitrogen.

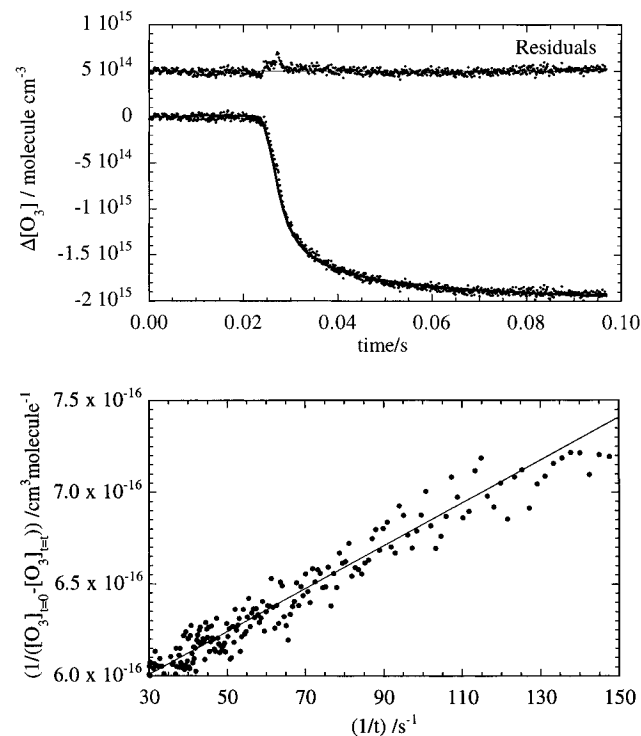


**Figure 5.** (a, top) Typical experimental trace of the change in ozone concentration following the photolysis flash (data points), with best-fit simulated trace from FACSIMILE (solid line). The residuals have been offset by  $+5 \times 10^{14}$  molecules  $\text{cm}^{-3}$ , for clarity. (b, bottom) Arithmetic analysis of the ozone concentration changes, after Sander and Watson.<sup>17</sup>

atoms formed in channel 1a. Thus, by coupling these results, the branching ratio of the BrO self-reaction was computed.

In addition, for experiments in ozone, the consumption of ozone by bromine atoms generated in channel 1a was also related to the branching ratio, providing a second check on this quantity. Again, both numerical integration and an analytical solution could be used to relate  $\alpha$  to the temporally varying ozone concentration. The latter analysis, after Sander and Watson,<sup>18</sup> gives

$$\frac{1}{\Delta[\text{O}_3]_t} = \frac{k_{1b}}{k_{1a}[\text{BrO}]_0} + \frac{1}{2k_{1a}[\text{BrO}]_0^2} \left(\frac{1}{t}\right) \quad (\text{vi})$$

where  $\Delta[\text{O}_3]_t$  is the change in ozone concentration at time  $t$  from that after the initial production of BrO ( $t = 0$ ). Thus, a plot of  $1/\Delta[\text{O}_3]_t$  vs  $1/t$  gives  $k_{1a}$  and the branching ratio. Both analyses are shown in Figure 5.

Results for the BrO self-reaction are summarized in Table 2 along with recent values taken from the literature. As can be seen, the values obtained in this study are in excellent agreement with those obtained from the recent study of Mauldin *et al.*,<sup>5</sup> who used a combined PMT/diode array system to measure  $k_{1b}$  and  $\alpha$ . Errors quoted refer to statistical scatter at the  $2\sigma$  level

and include a 10% uncertainty in the BrO cross sections, as reported by Wahner *et al.*<sup>27</sup>

At the limits of ozone concentration used in the  $\text{Br}_2/\text{O}_3$  photolysis system, some deviations from the simple kinetic scheme shown in Table 1 were noted. At very low ( $<10^{16}/\text{cm}^3$ ) ozone concentrations the phenomenological rate constant  $k_{\text{obs}}$  increased, although the BrO decay did not deviate from second-order. By analogy with chlorine, and as originally suggested by Bridier *et al.*,<sup>25</sup> this is attributed to the  $\text{Br} + \text{BrO}$  reaction, followed by the reaction of  $\text{Br}_2\text{O}$  and Br:

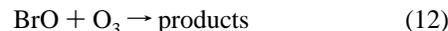


net:



These reactions, along with the  $\text{Br} + \text{Br} + \text{M}$  termolecular combination, effectively reduce the number of Br atoms available for reconversion back into BrO *via* reaction 2. The observed BrO loss rate is therefore enhanced due to a contribution from channel 1a. Given this proposed mechanism, any significant buildup of  $\text{Br}_2\text{O}$  would cause a deviation from second-order kinetics, but this was not observed.  $\text{Br}_2\text{O}$  has a strong absorption spectrum with two peaks around the wavelength region used in this work:<sup>28,29</sup> one at 200 nm with a cross section of  $2 \times 10^{-17} \text{ cm}^2 \text{ molecule}^{-1}$  and one at 314 nm with a peak cross section of  $2.3 \times 10^{-18} \text{ cm}^2 \text{ molecule}^{-1}$ . No evidence for  $\text{Br}_2\text{O}$  was observed in the residual spectra after removal of the BrO and  $\text{O}_3$  contributions, allowing an upper limit of  $1 \times 10^{13}$  molecules  $\text{cm}^{-3}$  to be placed upon its concentration. This result implies that the  $\text{Br} + \text{Br}_2\text{O}$  reaction is fast: no previous measurements of this reaction rate exist, but the chlorine analogue reaction  $\text{Cl} + \text{Cl}_2\text{O}$  is extremely rapid, with  $k_{298} = 9.9 \times 10^{-11} \text{ cm}^3 \text{ molecule}^{-1} \text{ s}^{-1}$ .<sup>30</sup> These findings were confirmed by adding reactions 10 and 11 to the reaction scheme for numerical integration and fitting using FACSIMILE. It was found that, provided that  $k_{11}$  was greater than  $k_{10}$  by a factor of 20, the simulated  $\text{Br}_2\text{O}$  concentration was always low ( $<10^{13}$  molecules  $\text{cm}^{-3}$ ) and the decay traces were well-described by the simulation. The returned values of  $k_{10}$  lay in the range  $(2-4) \times 10^{-12} \text{ cm}^3 \text{ molecule}^{-1} \text{ s}^{-1}$ , not inconsistent with the value reported by Hayman *et al.*<sup>31</sup> of  $1.9 \times 10^{-12} \text{ cm}^3 \text{ molecule}^{-1} \text{ s}^{-1}$ . Furthermore, the simulations were found to be very insensitive to  $k_{11}$ , above a lower limit of  $k_{11}$  of  $4 \times 10^{-11} \text{ cm}^3 \text{ molecule}^{-1} \text{ s}^{-1}$ .

At high ( $>10^{17}/\text{cm}^3$ ) ozone concentrations, some deviations from the second-order kinetic scheme were noted, which can be seen clearly in the second-order plot in Figure 6. This deviation is indicative of another reaction process for BrO, in addition to the second-order removal. The extent of the deviation from second-order was also found to increase with increasing ozone concentration. This behavior appears consistent with a contribution to the decay of BrO from the slow  $\text{BrO} + \text{O}_3$  reaction, giving products other than bromine atoms:



Reaction 12 was therefore incorporated into the reaction scheme for FACSIMILE to test this hypothesis. As can be seen from Figure 6, the agreement of the experimental and best-fit simulated BrO decays was somewhat improved when including  $\text{BrO} + \text{O}_3$ . Furthermore, the value of  $k_{12}$  returned from the simulation was independent of the ozone concentration used, supporting the hypothesis that the deviation from second-order is due to this channel. The average value of  $k_{12}$  obtained was

**TABLE 2: Measured Rate Constants and Comparison with Recent Previous Studies**

$k_1/10^{-12a}$	$k_{1a}/10^{-12a}$	$k_{1b}/10^{-13a}$	$\alpha$	number of determinations	source/reference
$2.98 \pm 0.42^b$		$4.68 \pm 0.68^b$		20	oxygen photolysis system
				10	bromine photolysis system:[BrO] monitoring
	$2.49 \pm 0.42^c$		$0.85 \pm 0.02^c$	10	bromine photolysis system:[O <sub>3</sub> ] monitoring
$2.78 \pm 0.24$		$4.45 \pm 0.82$	$0.84 \pm 0.01$	38	Mauldin <i>et al.</i> <sup>5</sup>
$3.1 \pm 0.4$				9	Bridier <i>et al.</i> <sup>25</sup>
$2.7 \pm 0.7$		$4.4 \pm 1.1$	$0.84 \pm 0.03$		DeMore <i>et al.</i> <sup>13</sup> (review)

<sup>a</sup> Units of  $\text{cm}^3 \text{ molecule}^{-1} \text{ s}^{-1}$ . <sup>b</sup> From analysis using FACSIMILE. <sup>c</sup> From graphical analysis.

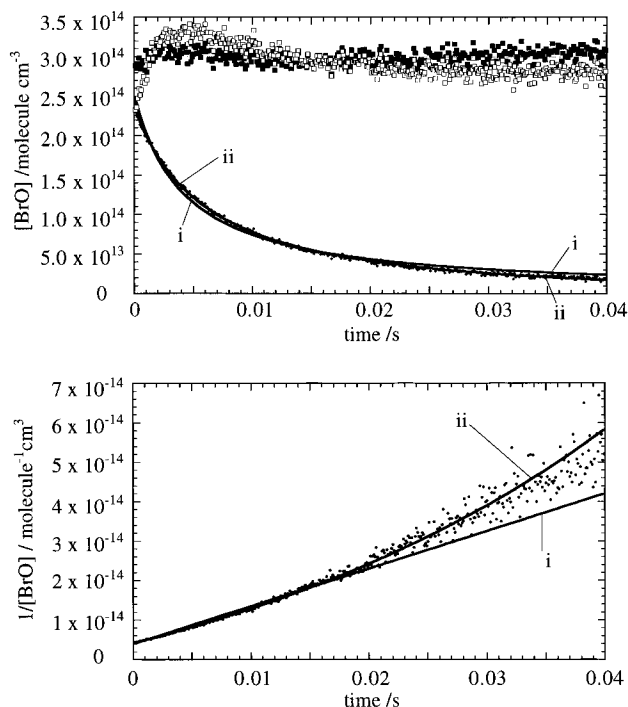


**Figure 6.** (a, top) Experimental BrO decay at high  $[\text{O}_3]$  (data points), with best fit FACSIMILE simulations using (i) pure second-order reaction scheme and (ii) reaction scheme including  $\text{BrO} + \text{O}_3 \rightarrow$  products. The residuals from both fits are shown, expanded  $\times 4$  and offset by  $+3.0 \times 10^{14} \text{ molecules cm}^{-3}$ , for clarity. Residual from simulation (i) = open symbols; residual from simulation (ii) = filled symbols. (b, bottom) Second-order plots of data and simulations from (a).

$(2.1 \pm 0.7) \times 10^{-17} \text{ cm}^3 \text{ molecule}^{-1} \text{ s}^{-1}$ , with  $k_{1b} = (4.57 \pm 0.80) \times 10^{-13} \text{ cm}^3 \text{ molecule}^{-1} \text{ s}^{-1}$  (errors are  $2\sigma$ ), which is in good agreement with the value obtained at lower ozone concentrations, wherein no deviation from second-order was observed. It is concluded that the reaction of BrO with ozone is playing a role in this reaction system at high ( $> 10^{17} \text{ molecules cm}^{-3}$ ) ozone concentrations.

The molecular products of reactions 1a and 1b were not quantified by UV spectroscopy, and no other products were observed in the wavelength range 234–367 nm in either the  $\text{O}_2$  or the  $\text{Br}_2$  photolysis system. However, recent work by Rattigan *et al.*<sup>32</sup> on the bromine photosensitized decomposition of ozone has identified the product OBrO and assigned its gas phase visible absorption spectrum for the first time. This spectrum extends from 400 to 600 nm and is highly structured, with pairs of absorption bands. A search for this absorber was therefore conducted in this work, as a potential reaction product. The wavelength region 425–558 nm was selected, again using the 150 grooves/mm grating. OBrO was not observed in the oxygen photolysis system, but experiments using bromine photolysis in ozone did show OBrO in the postflash spectra when ozone concentrations were high ( $> 1 \times 10^{17} \text{ cm}^{-3}$ ). Since

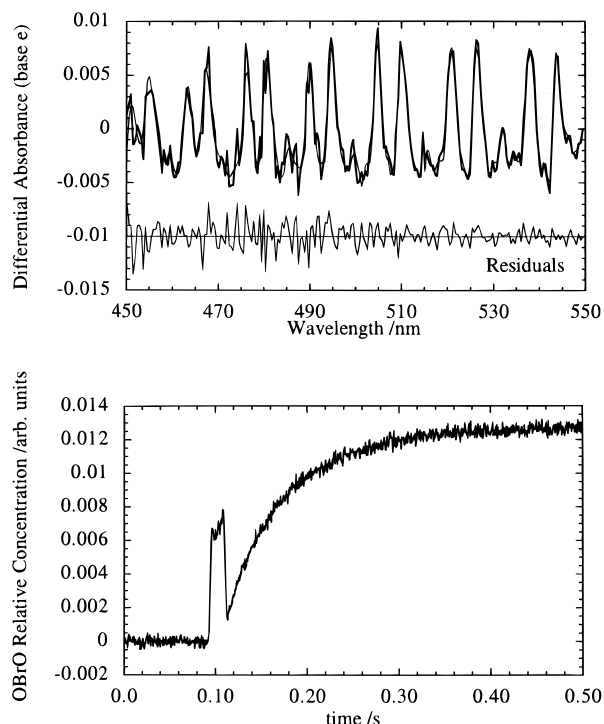


**Figure 7.** (a, top) Differential fit of a single postflash absorption spectrum (thick line) to the OBrO reference spectrum (fine line). The residuals have been offset by  $-0.01$  absorbance units, for clarity. Instrumental resolution =  $1.7 \text{ nm fwhm}$ . (b, bottom) Experimental trace of the buildup of OBrO.

the absolute absorption cross sections of OBrO have not been measured, the amount of OBrO evolved could not be determined. However, the differential fitting of a scaled relative spectrum to successive postflash spectra enabled the determination of the temporal variation of the relative OBrO amounts. Figure 7 shows a typical differential fit to the OBrO absorption and the temporal variation of the relative concentration.

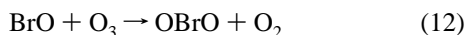
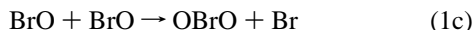
The relative amount of OBrO evolved was found to increase with increasing ozone concentrations over the range  $(1-7) \times 10^{17} \text{ cm}^{-3}$ . This strongly suggests that the OBrO could be a product of reaction 12. However, as Butkovskaya *et al.* report,<sup>33</sup> the reaction of bromine atoms with OBrO is fast ( $k_{13(298 \text{ K})} = 5 \times 10^{-11} \text{ cm}^3 \text{ molecule}^{-1} \text{ s}^{-1}$ ), and this effect could simply be a reflection of the lower steady state bromine atom concentration at the higher ozone concentrations:



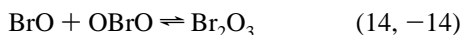
To determine the source of OBrO, experiments to monitor the formation of OBrO were carried out over ozone concentrations in the range  $(1-7) \times 10^{17} \text{ cm}^{-3}$ . At each ozone concentration, experiments were also carried out to monitor BrO, and FACSIMILE was used to model the results to attempt to establish which reaction was the source of OBrO. Since the

OBrO cross sections are unknown, the cross section values were assumed for the modeling on the basis of literature OCIO cross sections and the instrumental resolution used for this study. The assumed values related to a differential cross section of  $1 \times 10^{-17} \text{ cm}^2 \text{ molecule}^{-1}$  between the peak at 495.5 nm (corresponding to a  $(\nu_n, 0, 0) \leftarrow (0, 0, 0)$  symmetric stretch transition<sup>32</sup>) and the trough to short wavelengths at 491.1 nm, at the experimental instrumental resolution of 1.7 nm fwhm.

The FACSIMILE simulation was set up with OBrO either as a product of the BrO self-reaction (reaction 1c) or as a product of the BrO + O<sub>3</sub> reaction (reaction 12). However, it was found that neither system could adequately describe the evolution kinetics, because the OBrO formation occurred on a longer time scale than the BrO decay.



We therefore postulate here that an additional reaction of OBrO is taking place: the reversible combination with BrO to form Br<sub>2</sub>O<sub>3</sub>.



which is analogous to the ClO + OCIO reactions.<sup>34</sup> Although no absorption attributable to Br<sub>2</sub>O<sub>3</sub> was observed, the inclusion of reaction 14, -14 in the chemical scheme for integration did allow the observed behavior to be well-described by the simulation using either reaction 1c or 12 as the source of OBrO. However, in fixing the BrO self-reaction as the source of OBrO the value of  $k_{1c}$  returned was found to change markedly with ozone concentration. Conversely, when setting reaction 12 as the source of OBrO, the value obtained for the rate coefficient  $k_{12}$  was independent of the ozone concentration. This strongly suggests that the source of OBrO is reaction 12.

The averaged values of the rate coefficients  $k_{12}$ ,  $k_{14}$  and the equilibrium constant  $K_{14}$  obtained from FACSIMILE fitting for each simulation were

$$k_{12} = (1.66 \pm 0.11) \times 10^{-18} \text{ cm}^3 \text{ molecule}^{-1} \text{ s}^{-1}$$

$$k_{14} = (6.3 \pm 6.0) \times 10^{-11} \text{ cm}^3 \text{ molecule}^{-1} \text{ s}^{-1}$$

$$K_{14} = (4.2 \pm 4.0) \times 10^{-14} \text{ cm}^3 \text{ molecule}^{-1}$$

Errors are  $2\sigma$  and take no account of the systematic errors involved in the assumption of OBrO cross sections, which affect the returned value of  $k_{12}$  directly and inversely. Notwithstanding the large uncertainty in the value of  $K_{14}$ , a preliminary thermodynamic analysis was carried out to assess the feasibility of this equilibrium.<sup>35</sup> The values of  $S^0$  for OBrO and Br<sub>2</sub>O<sub>3</sub> were estimated from those of OCIO and Cl<sub>2</sub>O<sub>3</sub>, with adjustments made due to the difference in the translational partition function.<sup>35,36</sup> The resulting  $\Delta H^\circ$  obtained was  $-65.1 \text{ kJ mol}^{-1}$ , considerably more exothermic than that for the chlorine analogue compounds, for which  $\Delta H^\circ = -47.6 \text{ kJ mol}^{-1}$ .<sup>34</sup> Thus, although Br<sub>2</sub>O<sub>3</sub> is somewhat more stable than Cl<sub>2</sub>O<sub>3</sub>, the difference in enthalpies of formation is not unreasonable.

The values of the rate coefficients obtained from the analysis of the OBrO evolution kinetics were also used to simulate the variation with ozone concentration of the *maximum* OBrO concentration generated in each experiment. The results are shown in Figure 8, along with the observed variation (assuming the OBrO cross sections as discussed above) and that which is predicted from simulations in which reaction 1c was the source

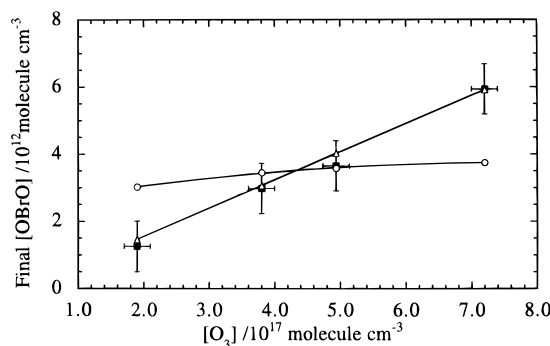


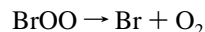
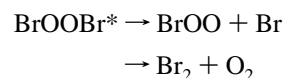
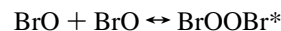
**Figure 8.** Final [OBrO] variation with ozone concentration (filled squares) and behavior predicted from simulations including OBrO formed in the BrO self-reaction (open circles) and OBrO formed in the BrO + O<sub>3</sub> reaction (open triangles).

of OBrO. As can be seen, the variation of the maximum relative [OBrO] generated is well-described by the mechanism using the BrO + O<sub>3</sub> source and not matched if OBrO is produced in the self-reaction, providing further confirmation of this finding.

Given the proposed secondary chemistry of OBrO, particularly the formation of Br<sub>2</sub>O<sub>3</sub>, the analysis of the BrO decay traces recorded at high [O<sub>3</sub>] deserves reconsideration. Should the BrO + O<sub>3</sub> reaction lead exclusively to OBrO, which then combines relatively rapidly with further BrO to produce Br<sub>2</sub>O<sub>3</sub>, the actual rate for the BrO + O<sub>3</sub> reaction will be 50% of that returned from the BrO decay kinetics. Furthermore, this rate is also based on the assumption that the deviation from second-order BrO decay kinetics is exclusively due to the BrO + ozone reaction producing non-bromine atom products: other first-order BrO loss processes could also contribute to this value. Given these assumptions, the value of  $2.1 \times 10^{-17} \text{ cm}^3 \text{ molecule}^{-1} \text{ s}^{-1}$  for the BrO + O<sub>3</sub> reaction rate should be taken as an upper limit.

Results for the analysis of the secondary chemistry at both low and high ozone concentrations are summarized in Table 3.

The results obtained for the individual reaction channels of the BrO self-reaction in this study show excellent consistency, regardless of the measurement used to derive values, and agree with the most recent determinations of the kinetics of this system.<sup>5,23-24</sup> The reaction products can be explained by the mechanism originally proposed by Porter,<sup>1</sup> involving the metastable BrOOBr intermediate. This species then forms unstable BrOO, which subsequently decomposes to form the atomic products or rearranges to form the molecular products.



The absence of OBrO as a product of the self-reaction suggests that the metastable BrOOBr\* intermediate does not form or rearranges to BrOOBr.

In reaction systems where insufficient ozone was present to scavenge bromine atoms, the termolecular Br + BrO + M addition reaction forms Br<sub>2</sub>O. It is followed in this system by the fast reaction of Br with Br<sub>2</sub>O to regenerate Br<sub>2</sub>, serving to convert bromine atoms into Br<sub>2</sub> and prevent buildup of Br<sub>2</sub>O, as observed. These reactions are analogous to those of the chlorine counterparts.<sup>13,37</sup> Some experimental evidence for the Br + Br<sub>2</sub>O reaction has since been observed by Orlando and Burkholder,<sup>28</sup> who observed BrO in the photolysis of Br<sub>2</sub> in the presence of Br<sub>2</sub>O.

**TABLE 3: Measured Rate Coefficients from Numerical Integration of Secondary Chemistry in the Br<sub>2</sub> Photolysis System**

reaction	$k_{(298\text{ K})}/\text{cm}^3 \text{ molecule}^{-1} \text{ s}^{-1}$	note
$\text{Br} + \text{BrO} \rightarrow \text{Br}_2\text{O}$	$(2-4) \times 10^{-12}$	a
$\text{Br} + \text{Br}_2\text{O} \rightarrow \text{BrO} + \text{Br}_2$	$>4 \times 10^{-11}$	a
$\text{BrO} + \text{O}_3 \rightarrow \text{products}$	$(2.1 \pm 0.7) \times 10^{-17}$	b
$\text{BrO} + \text{BrO} \rightarrow \text{Br}_2 + \text{O}_2$	$(4.57 \pm 0.80) \times 10^{-13}$	b
$\text{BrO} + \text{O}_3 \rightarrow \text{OBrO} + \text{O}_2$	$(1.66 \pm 0.11) \times 10^{-18}$	c
$\text{BrO} + \text{OBrO} \leftrightarrow \text{Br}_2\text{O}_3$	$(6.3 \pm 6.0) \times 10^{-11}$	c
	$K = (4.2 \pm 4.0) \times 10^{-14d}$	c

<sup>a</sup> In low [O<sub>3</sub>] (<10<sup>16</sup> cm<sup>-3</sup>) experiments only. <sup>b</sup> In high [O<sub>3</sub>] (>10<sup>17</sup> cm<sup>-3</sup>) experiments only, monitoring BrO. <sup>c</sup> In high [O<sub>3</sub>] (>10<sup>17</sup> cm<sup>-3</sup>) experiments only, monitoring OBrO and using assumed cross sections for OBrO (see text for details). <sup>d</sup> Units of cm<sup>3</sup> molecule<sup>-1</sup>. All errors quoted are 2σ and represent statistical scatter only.

In previous works, the products of the reaction of BrO with ozone have been assumed to be exclusively bromine atoms and molecular oxygen.<sup>5,17</sup> This results from the lack of any observed deviation from second-order kinetics in BrO decays recorded under conditions of excess ozone. In this work, such deviations have been observed, however, as a result of the increased signal-to-noise ratio afforded by the multiple wavelength monitoring. Furthermore, the identification of OBrO in experiments by Rattigan and Cox<sup>32</sup> provides a suitable candidate for other products of this reaction. Observation and modeling of the OBrO buildup have confirmed this, provided the OBrO undergoes reversible association with BrO to form Br<sub>2</sub>O<sub>3</sub>. Again, the analogous chlorine system is a precedent for this.<sup>34</sup> The absence of any absorption attributable to Br<sub>2</sub>O<sub>3</sub> could indicate that this product does not absorb in the wavelength regions used for these experiments, *i.e.* 234–367 and 425–558 nm, or that only a small quantity is formed that is below our detection limits.

The mechanism of OBrO formation in the BrO + O<sub>3</sub> reaction remains unclear. Turnipseed *et al.*<sup>23</sup> speculate that the formation of a weak adduct of BrO and O<sub>3</sub> at low temperatures explains the discrepancy between their results obtained for the BrO self-reaction using different radical sources. Further experiments as a function of pressure and temperature are needed to resolve this.

## Conclusions

A novel flash photolysis system has been developed using a charge-coupled device (CCD) detector. This represents the first such use of these devices in studies of gas phase kinetics and enables sequential absorption spectra to be recorded from the reacting mixture on microsecond time scales.

Preliminary studies of the BrO self-reaction have been carried out to demonstrate the capability of the system in kinetics studies. The recording of multiple wavelengths enables the simultaneous monitoring of several UV/visible absorbing components in the reaction mixture. In addition, the unequivocal and accurate quantification of species gives a high signal-to-noise ratio without the need for excessive experiments.

This study of the BrO self-reaction at 298 K is an independent, direct determination of both reaction channels. Results are in excellent agreement with previously published work. Some complications to the kinetics have been noted at extreme values of experimental ozone concentration used, including the observation and monitoring of the recently identified OBrO molecule. Our results indicate that this product is formed in the BrO + O<sub>3</sub> reaction and not the BrO self-reaction. This characterization of the secondary chemistry highlights the advantages of the CCD multiple wavelength monitoring: the data is of sufficient quality to enable the analysis of very small

deviations from the expected kinetic scheme, and the monitoring of a range of wavelengths allows the ready identification of additional reaction products.

The novel flash photolysis system described in this work should prove to be a useful tool for the study of other gas phase reactions of UV/visible absorbing species. This study of the BrO self-reaction demonstrates the viability of the technique and reveals hitherto undiscovered secondary chemistry of these important reactive species.

**Acknowledgment.** This work was supported by the NERC Atmospheric Chemistry Special Topic (Contract GST/02/877 A) and the EC Environment programme (Contract EV5V-CT93-338). We thank all of the technical staff at Cambridge University Chemistry Department who have participated in the apparatus development. We thank Oliver Rattigan and Tony Cox for the communication of results prior to publication and for several useful discussions. We thank Deb Fish for assistance with the analysis software development.

## References and Notes

- (1) Porter, G. *Proc. R. Soc. London Ser. A* **1950**, *200*, 284.
- (2) Norrish, R. W. G.; Porter, G.; Thrush, B. A. *Proc. R. Soc. London Ser. A* **1953**, *216*, 165.
- (3) Porter, G.; West, P. *Proc. R. Soc. Ser. A* **1964**, *279*, 302.
- (4) Sander, S. P.; Friedl, R. R. *J. Phys. Chem.* **1989**, *93*, 4764.
- (5) Mauldin, R. L., III; Wahner, A.; Ravishankara, A. R. *J. Phys. Chem.* **1993**, *97*, 7585.
- (6) Harwood, M. H.; Jones, R. L. *J. Geophys. Res.* **1994**, *99*, 22955.
- (7) Rattigan, O. V.; Rowley, D. M.; Wild, O.; Jones, R. L.; Cox, R. A. *J. Chem. Soc., Faraday Trans.* **1994**, *90*, 1819.
- (8) Dereniak, E. L.; Crowe, D. G. *Optical Radiation Detectors*; John Wiley & Sons: New York, 1984; Chapter 9.
- (9) Markiewicz, J. P.; Emmet, J. L. *J. Quantum Electron.* **1966**, *QE-2* (11).
- (10) Phillips, R. *Sources and Applications of Ultraviolet Radiation*; Academic Press Inc.: London, 1983.
- (11) Harwood, M. H.; Jones, R. L.; Cox, R. A.; Lutman, E.; Rattigan, O. V. *J. Photochem. Photobiol. A: Chem.* **1993**, *73*, 167.
- (12) Curtis, A. R.; Sweetenham, W. P. *FACSIMILE*, AERE Harwell publication R 12805; Computer Science and Systems Division, Harwell Laboratory: Oxfordshire, U.K., 1987.
- (13) DeMore, W. B.; Sander, S. P.; Golden, D. M.; Hampson, R. F.; Kurylo, M. J.; Howard, C. J.; Ravishankara, A. R.; Kolb, C. E.; Molina, M. J. *Chemical Kinetics and Photochemical Data for Use in Stratospheric Modeling*; JPL publication 92-20; California Institute of Technology: Pasadena, 1992.
- (14) Atkinson, R.; Baulch, D. L.; Cox, R. A.; Hampson, R. F.; Kerr, J. A.; Troe, J. *Evaluated Kinetic and photochemical Data for Atmospheric Chemistry—Supplement IV, IUPAC Subcommittee on Gas Kinetic Data Evaluation for Atmospheric Chemistry. J. Phys. Chem. Ref. Data* **1992**, *21*, 1125.
- (15) Scientific Assessment of Ozone Depletion, 1994. WMO Global Ozone Research and Monitoring Project, Report No. 37; World Meteorological Organisation: Geneva, 1994.
- (16) Barrie, L. A.; Bottenheim, J. W.; Schnell, R. C.; Crutzen, P.; Rasmussen, R. A. *Nature* **1988**, *334*, 138.
- (17) Sander, S. P.; Watson, R. T. *J. Phys. Chem.* **1981**, *85*, 4000.
- (18) Clyne, M. A. A.; Cruse, H. W. *Trans. Faraday Soc.* **1970**, *66*, 2214.
- (19) Basco, N.; Dogra, S. K. *Proc. R. Soc. London Ser. A* **1971**, *323*, 417.
- (20) Clyne, M. A. A.; Watson, R. T. *J. Chem. Soc., Faraday Trans. 1* **1975**, *71*, 336.
- (21) Jaffe, S.; Mainquist, W. K. *J. Phys. Chem.* **1980**, *84*, 3277.
- (22) Cox, R. A.; Sheppard, D. W.; Stevens, M. P. *J. Photochem.* **1982**, *19*, 189.
- (23) Turnipseed, A. A.; Birks, J. W.; Calvert, J. W. *J. Phys. Chem.* **1990**, *94*, 7477.
- (24) Lançar, I. T.; Laverdet, G.; LeBras, G.; Poulet, G. *Int. J. Chem. Kinet.* **1991**, *23*, 37.
- (25) Bridier, I.; Veyret, B.; Lesclaux, R. *Chem. Phys. Lett.* **1993**, *201*, 563.
- (26) Wahner, A.; Ravishankara, A. R.; Sander, S. P.; Friedl, R. R. *Chem. Phys. Lett.* **1988**, *152*, 507.
- (27) Atmospheric Ozone 1985. WMO Global Ozone Research and Monitoring Project, Report No. 16; World Meteorological Organisation: Geneva, 1985.

- (28) Orlando, J. J.; Burkholder, J. B. *J. Phys. Chem.* **1995**, *99*, 1143.
- (29) Rattigan, O. V. Private communication, 1995.
- (30) Burrows, J. P.; Cox, R. A. *J. Chem. Soc., Faraday Trans. 1* **1981**, *77*, 2465.
- (31) Hayman, G. D.; Danis, F.; Thomas, D. A. In Proceedings of Air Pollution Research Report 45: Chemical Mechanisms Describing Tropospheric Processes; Peeters, J., Ed.; CEC Publications: Leuven, Belgium, 1992.
- (32) Rattigan, O. V.; Jones, R. L.; Cox, R. A. *Chem. Phys. Lett.* **1994**, *230*, 121.
- (33) Butkovskaya, N. I.; Morozov, I. I.; Tal'Rose, V. L.; Vasiliev, E. *S. Chem. Phys.* **1983**, *79*, 21.
- (34) Burkholder, J. B.; Mauldin, R. L., III; Yokelson, R. J.; Solomon, S.; Ravishankara, A. R. *J. Phys. Chem.* **1993**, *97*, 7597.
- (35) Harwood, M. H. Ph.D. Thesis, University of Cambridge, 1995.
- (36) Benson, S. W. *Thermochemical Kinetics*, 2nd ed.; John Wiley and Sons: London, 1976.
- (37) Nickolaisen, S. L.; Friedl, R. R.; Sander, S. P. *J. Phys. Chem.* **1994**, *98*, 155.

JP951825B